Technical Report No. 332

Study of $\bar{p}p \to 4\pi^0$ in flight

D. Odoom and D.V. Bugg, QMWC, London

1 Abstract

From an analysis of $\bar{p}p \to 4\pi^0$ at a beam momentum of 1940 MeV/c, we find evidence for a $J^{PC} = 1^{++}$ resonance in 3π at 1640 $\pm 12(stat) \pm 20(syst)$ MeV with $\Gamma = 300 \pm 22 \pm 40$ MeV; it is observed decaying both to $\sigma\pi$ with $L = 1$ and to $f_2(1270)\pi$ with $L = 1$.

2 Physics Motivation

The motivation for this work was actually to look for a $\pi_2(1875)$ resonance as partner to the $\eta_2(1875)$ resonance found by Andy Cooper [1]. Since $\eta_2(1875)$ appears in the $\eta f_2(1270)$ channel, it seemed plausible to search for its partner in $\pi f_2(1270)$. In fact we have found NO evidence for such a resonance, so the motivation is of historical significance only!

In the standard quark model, there are several known $I = 1$ resonances around 1600-1700 MeV mass: $\rho_3(1690)$ (3^{--}), $\pi_2(1670)$ (2^{-+}), $\rho_1(1700)$ (1^{--}), $a_2(1660)$ (2^{++}), and $\pi(1740)$, $\pi(1800)$ (0^{-}) from VES [2]. Paul Eugenio [3] has also recently found evidence in E852 data for an $I = 0$ $J^{PC} = 1^{+-}$ resonance at 1540 MeV, decaying to $\omega\eta$. We shall present evidence for a 1^{++} resonance with $I = 1$ which fits neatly into the quark model in this mass region. There was some evidence for its $I = 0$ partner in the $\eta\pi\pi$ channel around 1700 MeV in Chris Pinder's data [4], although no precise determination of mass or width was possible.

A further group of $L = 3$ $\bar{q}q$ resonances up to $J^{PC} = 4^{++}$ is expected around $a_4(2050)$. We have searched for them, but not located any.

3 Processing of Data

This follows standard procedures in flight. Software versions used were:
CBOFF 1.29/00
LOCATER 2.00/00
CBKFIT 3.09/00
BCTRACK 2.00/03
GTRACK 1.21/09
CCDBCB 2.05/00
CBGEANT 5.04/00.
We have processed 4.12 $\times 10^6$ all-neutral triggers from August 1994. Cluster cuts were:
ECLUBC = 4.0 MeV, EPEDBC = 10.1 MeV, ECLSBC = 4.0 MeV.
The event selection demanded the absence of charged tracks and the pile-up flag; the error code for reconstruction was 0, total momentum < 150 MeV/c, and total energy > 2200 MeV; the total available centre of mass energy is 2409 MeV. Pull quantities had sigmas of 0.85–1.0 times predictions.

Events containing exactly 8γ were first fitted to $\bar{p}p \to 8\gamma$, demanding a confidence level (CL) $> 1\%$. Split-offs were discarded. The maximum split-off energy was 100 MeV, and the minimum energy for an accepted γ was 10 MeV. We required unambiguous pairing of photons to make $4\pi^0$ and a kinematic fit with CL $> 10\%$. Wrong combinations of photons are estimated at 3.3% from the Monte Carlo simulation. Backgrounds were rejected if any of the following were fitted with CL $> 0.5\%$: (i) $3\pi^0\eta$ or $\eta\eta\pi^0\pi^0$, (ii) $\omega\omega\pi^0$, $\omega \to \pi^0\gamma$; (iii) 1294 $\eta\pi^0$, $\eta \to 3\pi^0$ events were eliminated by applying a cut at a $3\pi^0$ mass of 600 MeV/c^2.

The $4\pi^0$ channel is quite prolific and backgrounds from other channels are low. A Monte Carlo study using GEANT shows that the largest background is from $\eta\pi^0\pi^0\pi^0$ and is $< 1\%$. Another possible background arises from 9γ events ($\omega\pi^0\pi^0\pi^0$ and $\omega\eta\pi^0\pi^0$) where one photon is lost; however, a search in the data for $\omega \to \pi^0\gamma$ reveals no signal at the 0.7% level. This is illustrated in Fig. 1.

After kinematic fitting to $\bar{p}p \to 4\pi^0$, the data sample consists of 26,587 events. The maximum likelihood analysis described below uses 84,967 Monte Carlo events simulating the acceptance of the detector and satisfying identical selection criteria to data.

We define log likelihood as follows:

$$S = (\sum_{j=1}^{N} \ln w_j) - N(\sum_{i=1}^{M} \ln w_i). \qquad (1)$$

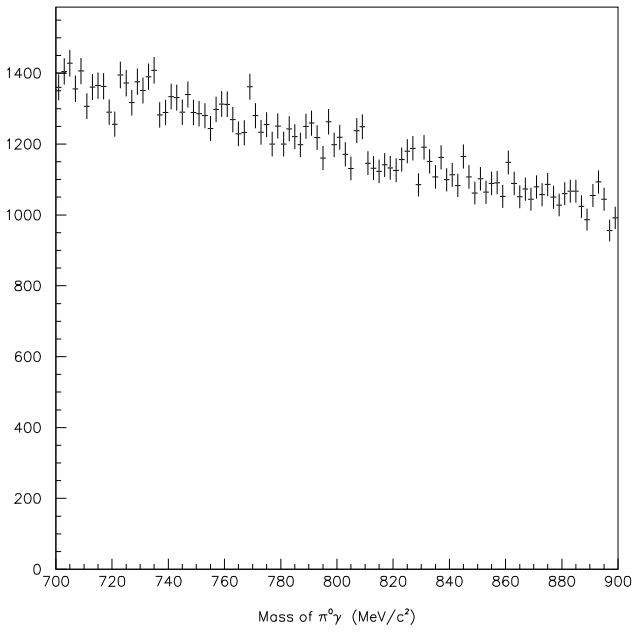

Fig. 1. The $\pi^0\gamma$ mass spectrum from all combinations.

Here N is the number of events, M the number of Monte Carlo events, and w is the cross section for the kinematics of a particular event. With this definition, a change of log likelihood of 0.5 corresponds to 1 standard deviation.

4 Features of the Data

Fig. 2 shows projections and scatter plots. They show evidence for $f_2(1270)$, but rather little else. In the $3\pi^0$ mass^2 projection, Fig. 2(b), there is a distinct shoulder at about $s = 4.6$ GeV^2. Full histograms on Figs. 2(a) and (b) are from the maximum likelihood fit. Figs. 2(e) and (f) are scatter plots from the fit, for comparison with Figs. 2(c) and (d).

5 Amplitude Analysis

The main channels contributing to the data are:

$$\bar{p}p \to \sigma\sigma \tag{2}$$
$$\to f_2(1270)\sigma \tag{3}$$

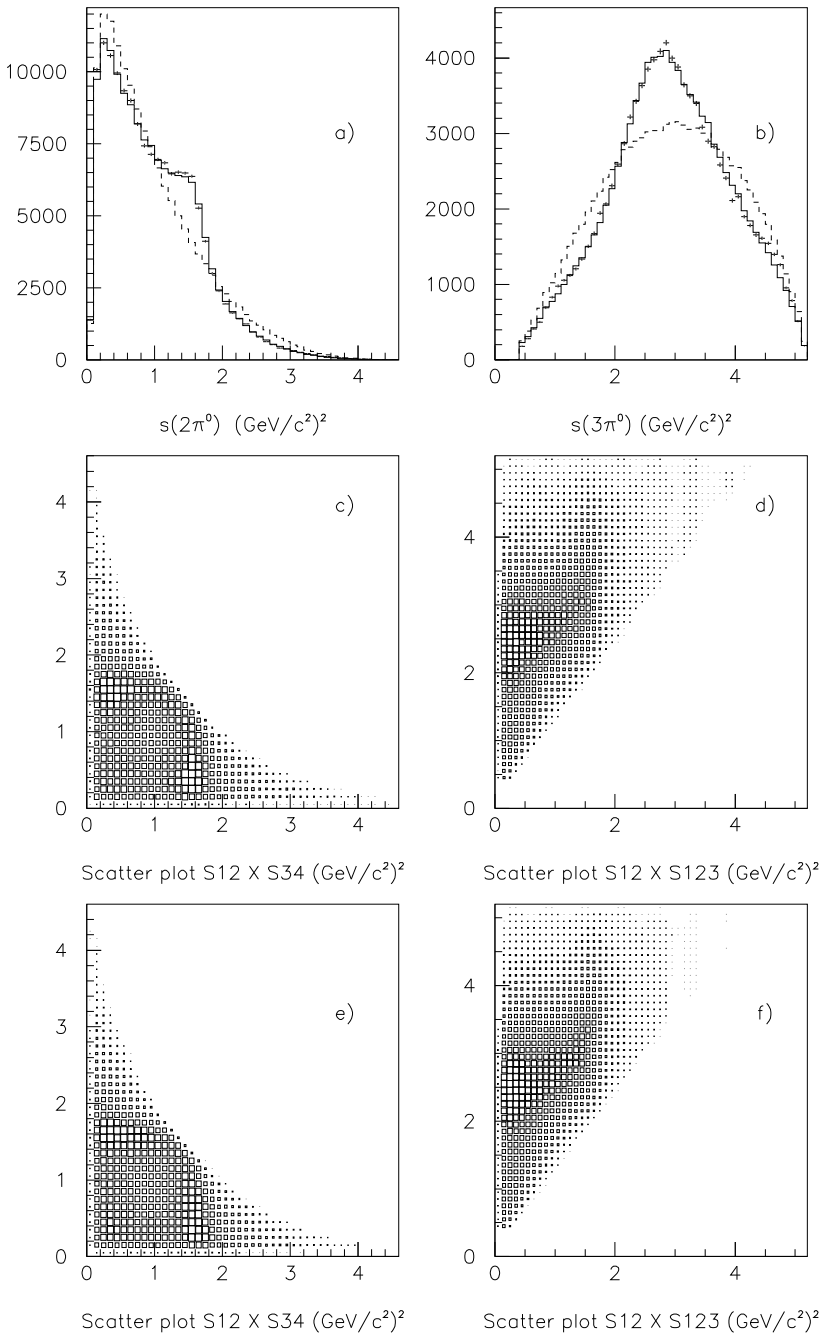

Fig. 2. (a) $2\pi^0$ spectrum, (b) $3\pi^0$ spectrum; full histograms show the fit. The dashed histograms show phase space folded with detector acceptance. The vertical scale shows numbers of combinations. Scatter plots for data: (c) s_{12} v. s_{34}, (d) s_{12} (horizontally) v. s_{123} (vertically); (e) and (f) are scatter plots for the fit, to be compared with (c) and (d) respectively.

$$\to f_2(1270)f_2(1270) \tag{4}$$
$$\to \pi_2(1670)\pi,\ \pi_2 \to [f_2(1270)\pi]_{L=0} \tag{5}$$
$$\to \pi_2(1670)\pi,\ \pi_2 \to [\sigma\pi]_{L=2}. \tag{6}$$

Here L is the orbital angular momentum in the decay of the resonance and σ is shorthand for the $\pi\pi$ S-wave amplitude; we use a slightly updated version of the parametrisation of Zou and Bugg [5]. Figs 3–7 show projections and scatter plots from each of channels (2)–(6) individually. The one closest to the data is $f_2(1270)\sigma$, and this channel does indeed give the largest contribution to the fit. Figs. 8-10 show projections and scatter plots from further channels:

$$\bar{p}p \to a_1(1640)\pi,\ a_1(1640) \to [\sigma\pi]_{L=1}, \tag{7}$$
$$\to a_1(1640)\pi,\ a_1(1640) \to [f_2(1270)\pi]_{L=1}, \tag{8}$$
$$\to \pi(1690)\pi,\ \pi(1690) \to [\sigma\pi]_{L=0}. \tag{9}$$

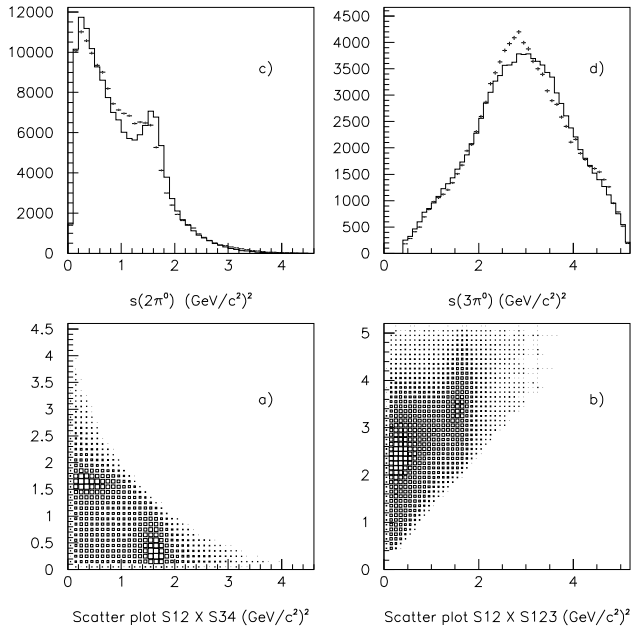

Fig.3 Scatter plots and projections from $f_2(1270)\sigma$.

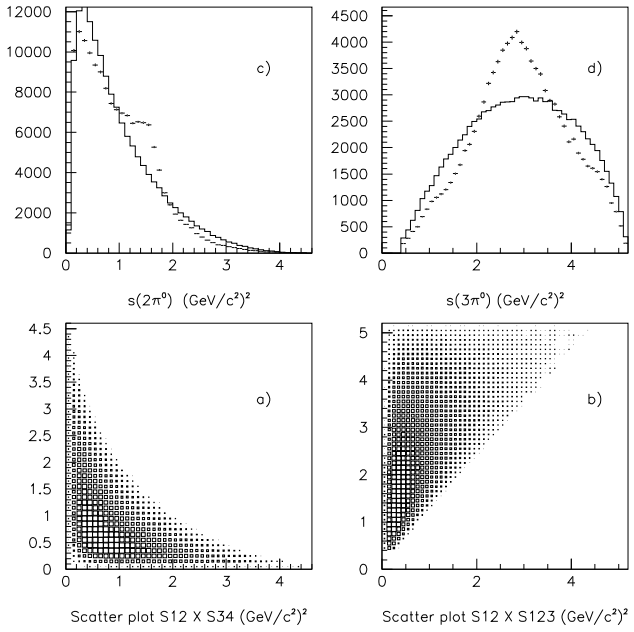

Fig.4 Scatter plots and projections from $\sigma\sigma$.

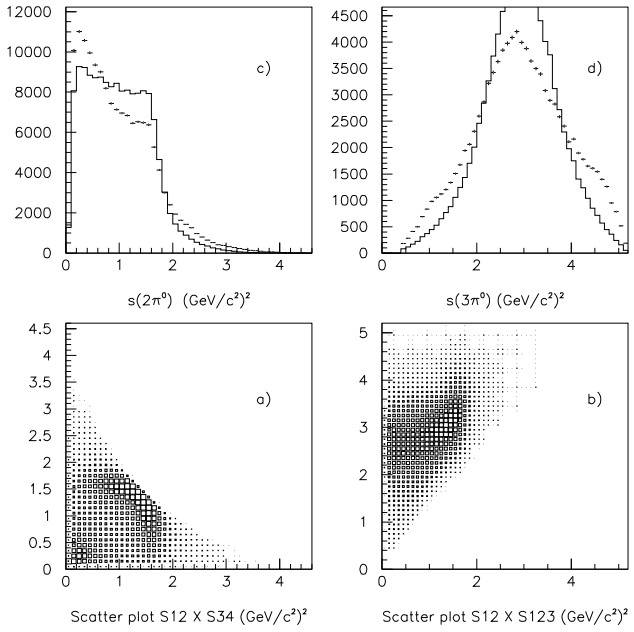

Fig. 5 Scatter plots and projections from $f_2(1270)f_2(1270)$.

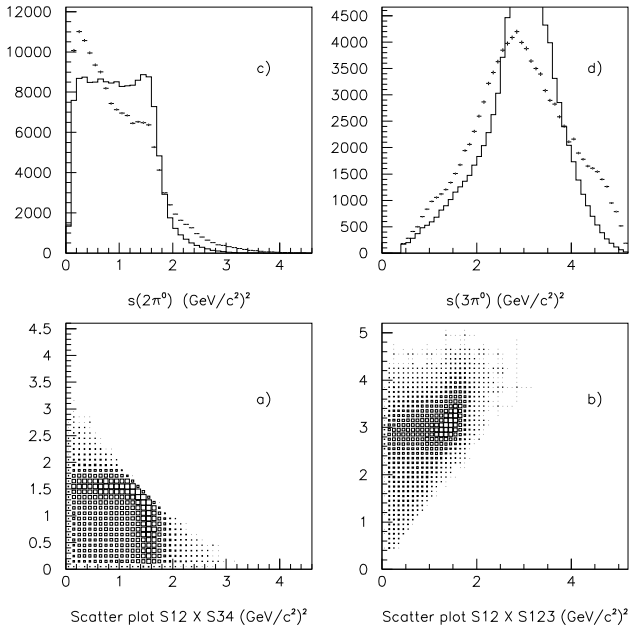

Fig.6 Scatter plots and projections from $\pi_2(1670) \to f_2(1270)\pi$.

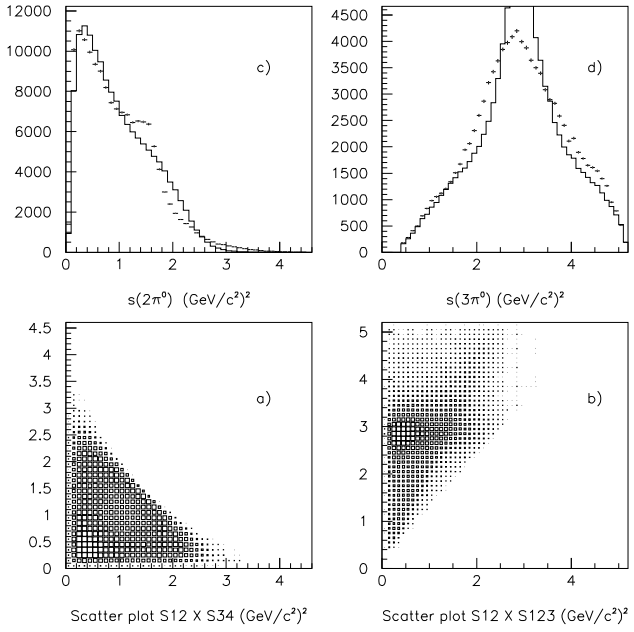

Fig.7 Scatter plots and projections from $\pi_2(1670) \to [\sigma\pi]_{L=2}$.

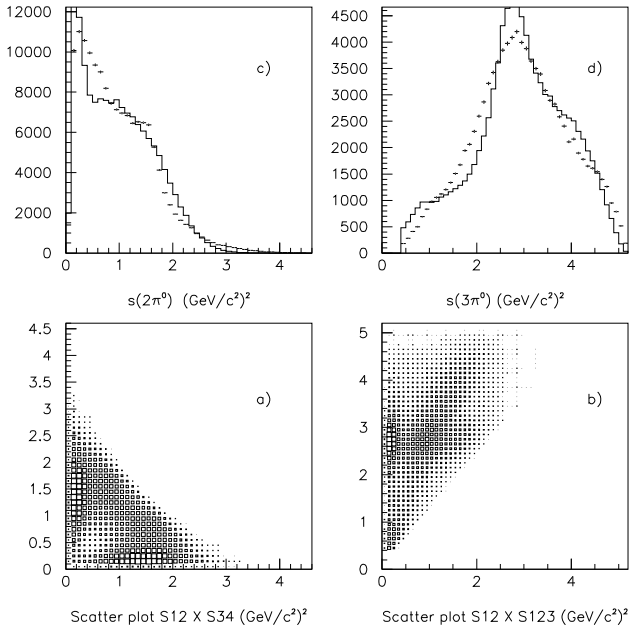

Fig.8 Scatter plots and projections from $a_1(1640) \to [\sigma\pi]_{L=1}$.

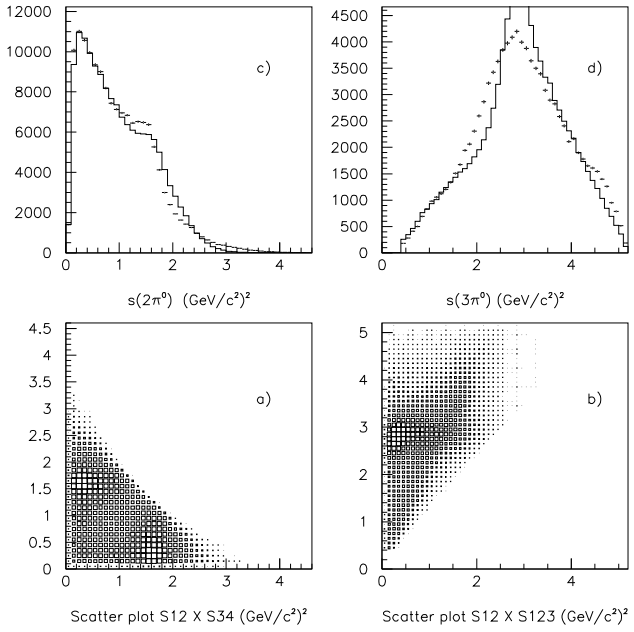

Fig.9 Scatter plots and projections from $a_1(1640) \to [f_2(1270)\pi]_{L=1}$.

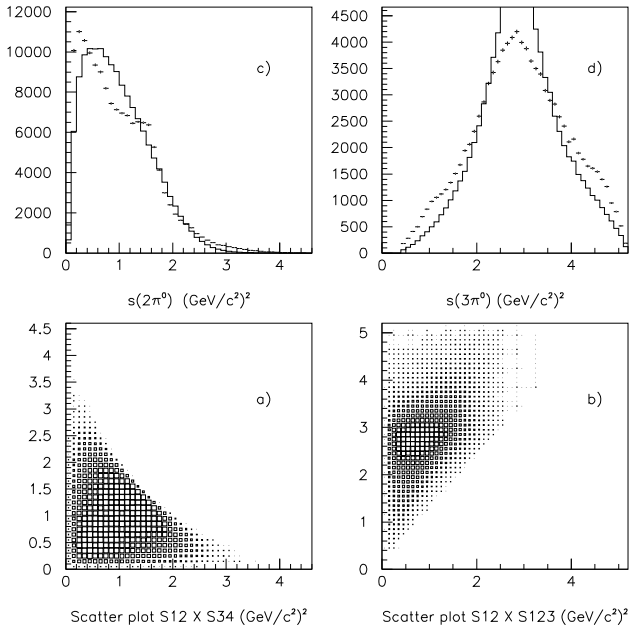

Fig.10 Scatter plots and projections from $\pi(1690) \to \sigma\pi$.

6 The Wick Rotation

The amplitude analysis follows the methods of Ref. [1]. There are too many partial waves to fit both production and decay. We fit the decays in full, since they give the primary information for spin-parity analysis of resonances. No attempt is made to fit the production process. Let us take as examples channels (5) and (6) with particles 1,2,3 making the π_2 and particles 12 the f_2 into which it decays. Suppose the π_2 of channel (5) is produced with component of spin m along the beam direction. The amplitude for its production is written

$$f_m = \frac{G_m \exp(i\delta) Y_2^m(\alpha, \beta)}{(M^2 - s_{123} - iM\Gamma)(m^2 - s_{12} - im\gamma)}. \tag{10}$$

Here G_m is a coupling constant and δ a phase for production of this channel; M, Γ refer to the mass and width of the π_2, and m, γ are the mass and width of the f_2. The Y are spherical harmonics in terms of polar angle α illustrated in Fig. 11 and azimuthal angle β around the beam direction. They are the decay angles of $f_2 \to \pi^0\pi^0$ with respect to the beam direction after two Wick rotations. The details of the Wick rotation are given in Ref. [1]. In outline, the steps are as follows. Particle momenta are first transformed to the centre

of mass frame. In general, the Wick rotation then consists of three steps: (i) a rotation through polar angle τ and azimuth ϕ to the direction of production of the $X \equiv \pi_2$; (ii) a Lorentz boost to its rest frame; (iii) a rotation back again through angles $-\phi$ and $-\tau$ in the rest frame of the π_2. The effect of the second rotation is to cancel the quantum mechanical rotation matrices required for the first rotation. Amplitudes are invariant under the boost to the rest frame of the resonance. A second Wick rotation is then made using angles γ, ϵ at which the f_2 appears after the first Wick rotation. The surviving spin dependence is simply given by $Y_2^m(\alpha, \beta)$ in equn. (10). For channel (6), $Y_2^m(\alpha, \beta)$ of equn. (10) is replaced by $Y_2^m(\gamma, \epsilon)$ describing the decay with $L = 2$ to $\sigma\pi$. Amplitudes for $-m$ are related to those for $+m$ by complex conjugation:

$$Y_2^1 = -[Y_2^{-1}]^*,$$
$$Y_2^2 = [Y_2^{-2}]^*.$$

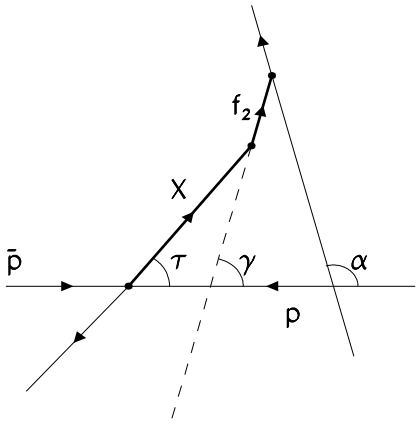

Fig.11 Angles used in the Wick rotation.

Amplitudes are summed coherently over all combinations of π^0. For channels (5) and (6), there are 12 such combinations; for $\sigma f_2(1270)$, there are 6 and for $\sigma\sigma$ there are 3. Cross sections are summed incoherently over m values. We allow partial interferences, because channels may be fed from a variety of initial partial waves. Interferences between channels (2)–(9) are all examined individually. The ones which are kept are those where log likelihood improves by more than 2 standard deviations, summed over m values. Only a modest number survive, but in almost all of these the interference effects are highly significant.

For both $\pi_2(1670)$ decay modes, the ratios of $m = 1$ and $m = 0$ amplitudes are constrained to be the same; likewise for both $a_1(1640)$ decay modes. For

$a_1(1640)$, the combined $m = \pm 1$ branching ratio dominates by a factor 3 over $m = 0$.

Table 1 shows changes in log likelihood when each channel is dropped from our final fit and the remaining channels are re-optimised. It also shows branching ratios for each channel, keeping interferences between combinations within the channel. These branching ratios do not add up to 100% because of interferences between channels. It is obvious from the first 5 entries of Table 1 that all of reactions (2)–(6) make substantial contributions and are required.

Channel	$\Delta(ln\ L)$	Branching fraction(%)
$\sigma\sigma$	437	28.2
$\sigma f_2(1270)$	698	43.8
$f_2(1270)f_2(1270)$	630	22.4
$\pi_2(1670) \to [f_2(1270)\pi]_{L=0}$	310	20.7
$\pi_2(1670) \to [\sigma\pi]_{L=2}$	271	6.2
$\pi_2(1670) \to [f_2(1270)\pi]_{L=2}$	12.6	0.7
All $\pi_2(1670)$	508	27.7
$a_1(1640) \to [\sigma\pi]_{L=1}$	79.0	10.2
$a_1(1640) \to [f_2(1270)\pi]_{L=1}$	20.5	2.8
Both $a_1(1640)$	152.0	13.0
$a_1(1260) \to [\sigma\pi]_{L=1}$	28.5	5.0
$\pi(1690)$	72.7	5.9

Table 1
Changes in log likelihood when each channel is dropped from the fit; also branching fractions including interferences within each channel, but excluding interferences between different channels.

7 Scanning

The shoulder at $M = 2.1$ GeV in Fig. 2(b) attracted our attention. This is close to the mass of $a_4(2050)$ and it seemed possible that this resonance and others with $J^P = 3^+$ or 2^+ might be responsible. To check this, we added to the amplitude analysis further $3\pi^0$ resonances one by one with all J^P from 0^- to 4^+; all possible L values were tried with decays to $\sigma\pi$ or $f_2(1270)\pi$. Each trial resonance was assigned a width of 250 MeV and its mass was scanned in 40 MeV steps from 1600 to 2300 MeV. None showed any optimum near 2.1 GeV.

The explanation which emerges for the shoulder is that it is due to a triple interference between three $f_2(1270)$ combinations in one group of $3\pi^0$. For three such resonances amongst particles 12, 23 and 13,

$$s_{123} = s_{12} + s_{23} + s_{13} - 3m_\pi^2 = 4.78\ GeV^2. \tag{11}$$

The triple interference is illustrated below for the $3\pi^0$ mass range 2025-2205 MeV in Fig. 20. When one allows further for the available $4\pi^0$ phase space, it gives a good description of the shoulder.

8 The $a_1(1640)$

The scans did, however, reveal a surprisingly strong 1^+ signal at 1640 MeV. It displays quite large interference with the channel $f_2(1270)\sigma$; this interference improves the fit by 24.4 in log likelihood. The width of the resonance optimises at 300±22 MeV, as shown in Fig. 12, with a systematic error which we estimate as ±40 MeV from variations over a wide choice of components in the fit. Fig. 13 shows the variation of log likelihood with the mass of this resonance for decays separately to $\sigma\pi$ (dashed curve) and $[f_2(1270)\pi]_{L=1}$ (dotted). The full curve shows the fit including both decay channels. Fig. 14 shows corresponding curves for other quantum numbers. [A technicality is that Blatt-Weisskopf centrifugal barriers are included for decays with a radius of 0.8 fm; in practice their effects are very small].

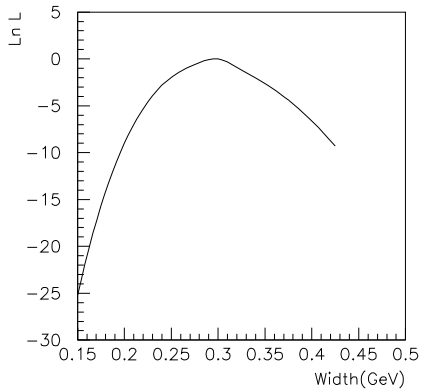

Fig.12 Illustrating the optimisation of the width of the 1^+ signal. The zero of the scale is taken at the optimum.

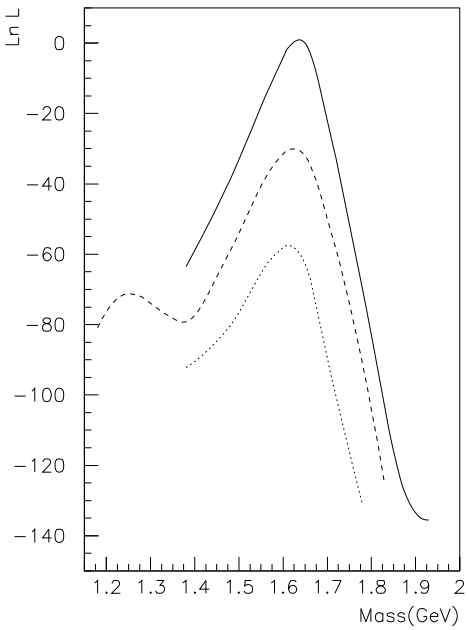

Fig.13 Log likelihood v. mass for a 1^+ resonance of width 300 MeV, decaying to $\sigma\pi$ (dashed) or $f_2(1270)\pi$ with $L = 1$ (dotted); the full curve shows the result with both included.

The obvious question is whether this peak may be due to cross-talk with $\pi_2(1670)$. To study this possibility, we have used the Monte Carlo events to generate several data samples weighted with the cross section we fit to channels (2)–(6). These data samples have then be fitted including in addition the 1^+ channels. In all cases, the fitted 1^+ signal is $< 1\%$. There is no peak in log likelihood at 1640-1670 MeV. So cross-talk with $\pi_2(1670)$ definitely does not explain the 1^+ peak.

A second check has been made that the data really have the angular dependences expected for 1^+ decays. Taking as an example the $\sigma\pi$ decay, the $m = 0$ amplitude is proportional to $\cos\gamma$ and the $m = 1$ amplitude is proportional to $\sin\gamma\exp(i\epsilon)$. We have replaced the angles γ, ϵ with a variety of other angles, e.g. τ, α, β and corresponding angles for the $f_2\sigma$ and f_2f_2 channels. In all cases, the peak in log likelihood drops dramatically to a height typically 25, and log likelihood gets worse by typically 100. Table 2 gives details of all these trials. As a crude measure of the height of the peak, the final column shows the difference in log likelihood at $M = 1635$ MeV from the mean of the values at the ends of the scan. The mean of the trials is shown in Fig. 15, compared with the mass scan for the correct angular dependence. It is clear that the

data do have the angular dependence characteristic of 1^+, even though this cannot be displayed directly because of the 12 combinations. The small peak which survives in entries 2–8 of Table 2 probably arises from the fact that 3-body phase space peaks near 1650 MeV.

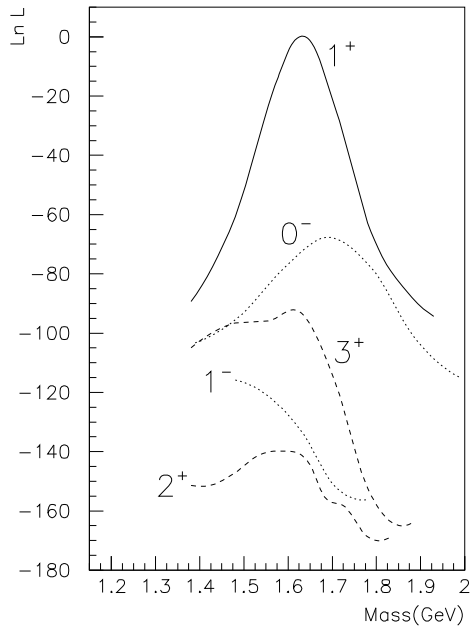

Fig.14 Log likelihood v. mass for (a) a 3^+ resonance of width 300 MeV with both $\sigma\pi$ and $f_2\pi$ decay modes; (b) 2^+ decaying to $f_2\pi$ with both $L = 1$ and $L = 3$; (c) 1^- decaying to $f_2\pi$ with $L = 2$; (d) $0^- \to \sigma\pi$. The full curve shows the fit including both decay modes of $a_1(1640)$ and also $a_1(1260)$ with PDG mass and width.

In Fig. 14, there are only very weak effects for 2^+ and 1^- (exotic). For 3^+ there is a distorted peak close to 1640 MeV, but with much poorer log likelihood than for 1^+. The lowest 3^+ resonance is to be expected in the $L = 3$ $q\bar{q}$ excitation around 2040 MeV so a 3^+ resonance near 1650 MeV is unlikely. We have found that the observed 3^+ peak may be explained as cross-talk with 1^+. This has been demonstrated by using the Monte Carlo events to generate data samples weighted with the cross section we fit to channels (2)–(8). These data samples have then been fitted with 3^+ replacing 1^+, and scanning the mass of the 3^+ component. This reproduces the 3^+ curve of Fig. 14 rather well. What is happening is that the detection efficiency of the detector drops close to the beam direction because of entrance and exit holes for the beam

Angles	$M = 1380$	$M = 1480$	$M = 1635$	$M = 1780$	$M = 1880$	Peak
$(\gamma\epsilon)(\alpha\beta)$	66.3	41.0	0	83.0	124.3	95.3
$(\alpha\beta)(\gamma\epsilon)$	136.2	131.3	117.5	148.1	155.2	28.2
$(\beta\alpha)(\epsilon\gamma)$	132.5	119.4	106.9	129.9	140.0	29.3
$(\alpha_2\beta_2)(\alpha_3\beta_3)$	143.7	143.2	133.6	149.0	154.5	15.5
$(\alpha_3\beta_3)(\alpha_2\beta_2)$	133.6	132.0	119.5	137.3	139.0	17.7
$(\beta_2\eta)(\beta\gamma)$	129.7	124.0	115.3	137.0	148.4	23.7
$(\epsilon\gamma)(\beta\alpha)$	98.1	77.0	72.3	128.6	132.4	37.9
$(\epsilon\gamma)(\eta\beta)$	103.7	94.8	88.0	137.4	143.7	35.7

Table 2
Values of $-\ln\ L$ v. the mass (MeV) of the a_1 for various choices of angles, and normalised to zero at the optimum. Entry 1 is the correct choice and all others are spurious. Angles α_2, β_2 correspond to α, β for the f_2 in $f_2\sigma$ and α_3, β_3 for the σ. The column labeled 'Peak' is the differencce between $M = 1635$ MeV and the mean of $M = 1380$ and $M = 1880$ MeV.

and cabling. The $Y_3^m(\gamma, \epsilon)$ dependence for 3^+ has similarities with Y_1^m for 1^+, and the loss of detection efficiency near $\cos\gamma = \pm 1$ allows 3^+ to simulate 1^+ to some extent.

When 3^+ alone is fitted to the data, its magnitude is 6.4%, compared with the simulation which predicts 5.9%. However, if both 1^+ and 3^+ are fitted to the data (with the same mass and width), most of the signal is fitted as 1^+ (12.7%) and only 2.1% is fitted as 3^+. Again this agrees closely with the simulation. We are therefore confident that the correct quantum numbers are 1^+, and that the 3^+ peak is an artefact.

This is a strong warning that we have to be alert for such confusion elsewhere. A dangerous situation arises if one restricts the fitted angular momenta, as in the above case fitting with 3^+ but no 1^+. The remedy seems to be to allow all plausible angular momenta, and the fit will choose the right one, though it admits some noise into absent channels (3^+ here). It is not really necessary to use GEANT to study this effect. We have studied it extensively with a simple Monte Carlo which generates four-vectors of events and enforces a hole around the beam upstream and downstream. We have found that cross-talk increases roughly as the area of the holes up to the point where the first Legendre zero is encountered; thereafter it becomes very serious.

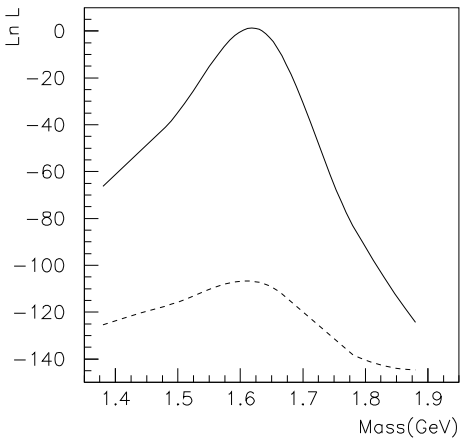

Fig.15 Log likelihood v. mass for the mean of 7 trials when the wrong angular dependence is substituted for 1^+ decays (dashed), compared with the fit (full curve) with the correct angular dependence, but without $a_1(1260)$ in the fit.

Fig. 14 also shows an optimum for 0^- at 1690 MeV. It is a possibility that this is due to a 0^- peak near this mass observed by the VES group at 1740 MeV [2]. However, we find that the height of the 0^- peak is strongly correlated with $\pi_2(1670) \to \sigma\pi$; any changes made to that channel or limitations on its branching ratio are transferred to strong changes in the 0^- peak. That is, there is cross-talk between 2^- and 0^-. Simulation shows that this accounts for roughly half of the 0^- peak of Fig. 14. For quantum numbers 0^- there is no angular dependence, and there is the further possibility of confusion with $\sigma\sigma$. Therefore we are not confident that the 0^- peak corresponds to real physics. With it included in the fit, the 1^+ signal optimises at 1635 MeV; with it excluded, the optimum is at 1650 MeV. We assign a compromise mass of 1640 MeV to the 1^+ signal, with a statistical error of ± 12 MeV and a systematic error of ± 20 MeV.

The scan for $1^+ \to \sigma\pi$ of Fig. 13 has been extended down to 1150 MeV, in order to search for $a_1(1260)$. According to the Particle Data Tables [6], the decay of $a_1(1260)$ to $\sigma\pi$ is extremely weak, with a branching ratio 0.003 ± 0.003. We do observe a small enhancement near the $a_1(1260)$, but cannot assign a branching ratio for lack of normalisation to other decay modes. Including $a_1(1260)$ improves ln L by 28.5, a suggestive amount, but not definitive. In our final fit, $a_1(1260)$ is included with PDG mass and width; it has little effect on the evidence for $a_1(1640)$, as shown by the full curve on Fig. 14. We have

likewise searched for $\pi(1300)$ but found no significant evidence for its presence.

9 Goodness of Fit

Fig. 16 shows mass projections with and without $a_1(1640)$ in the fit; there is hardly any discernable difference. Figs. 17–20 show Dalitz plots for intervals of $3\pi^0$ mass. These are all fitted adequately and none displays the presence of $a_1(1640)$. For comparison, Fig. 21 show fits with $a_1(1640)$ omitted. There is no visible effect in any of the mass ranges. Figs. 22-24 show projections from Figs. 17-21. There is a tiny effect visible for 1620 ± 45 MeV, but not enough to be convincing by itself.

We have used the PDG mass and width for $\pi_2(1670)$. Log likelihood shows a very small, but barely significant improvement if the mass and width are optimised. The optimum mass is 1692 ± 12 MeV, to be compared with the latest E852 value of 1683 ± 4 MeV from $\rho\pi$ decays.

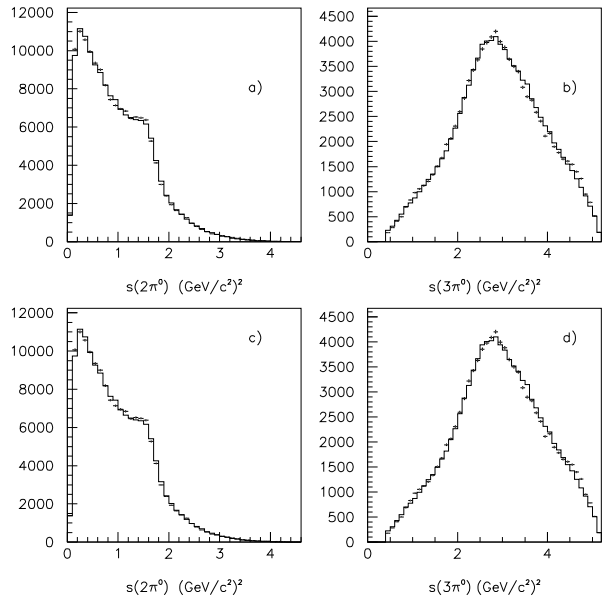

Fig.16 Mass projections (a) and (b) with and (c) and (d) without $a_1(1640)$ in the fit.

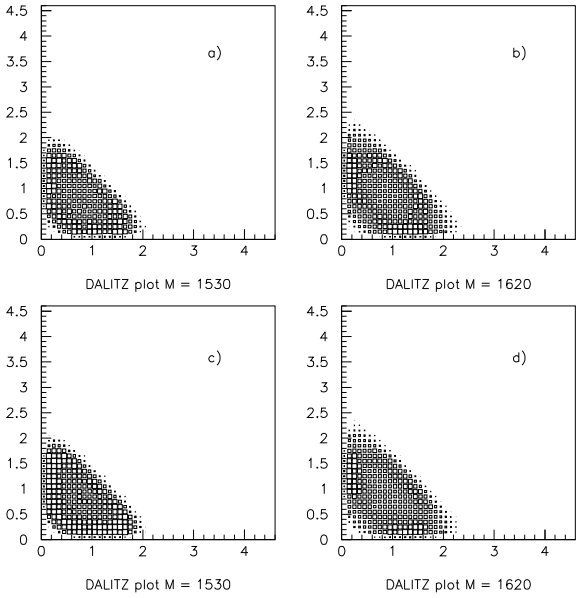

Fig.17 Dalitz plots (a) and (b) for data with $3\pi^0$ combinations within the mass ranges 1530 ± 45 MeV and 1620 ± 45 MeV, compared with the fit (c) and (d).

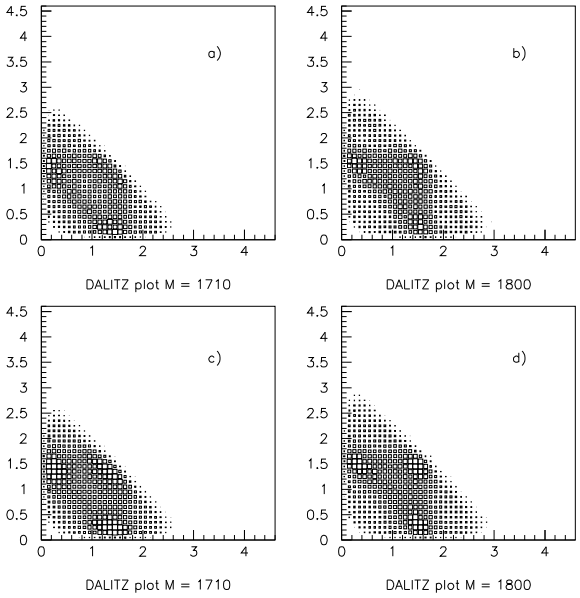

Fig.18 As Fig. 17 for $3\pi^0$ masses 1710 ± 45 and 1800 ± 45 MeV.

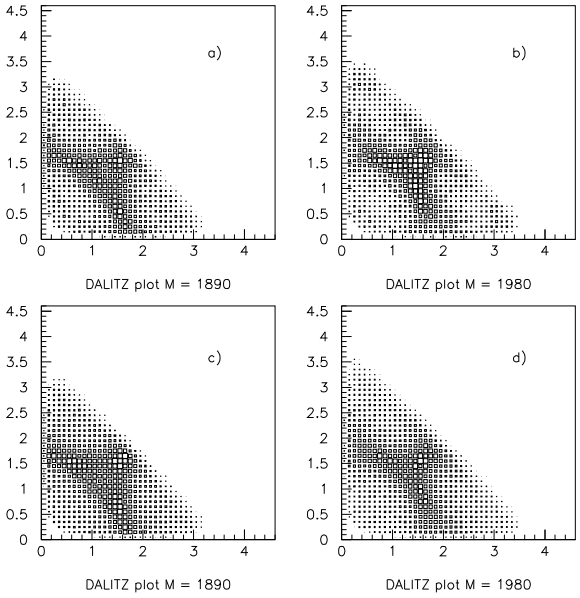

Fig.19 As Fig. 17 for $3\pi^0$ masses 1890 ± 45 and 1980 ± 45 MeV.

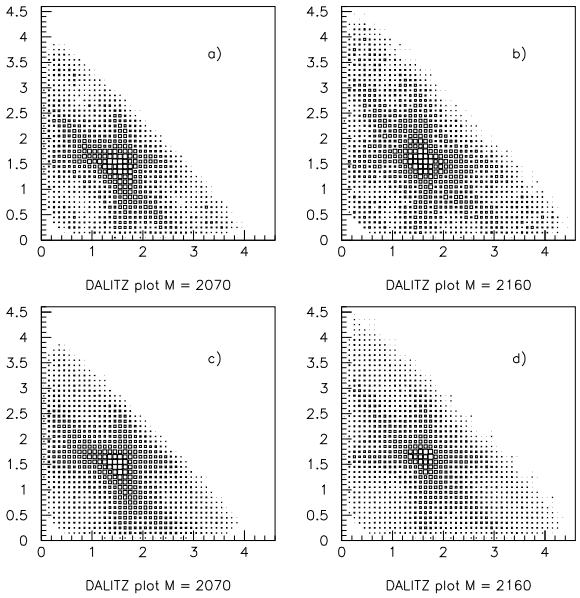

Fig.20 As Fig. 17 for $3\pi^0$ masses 2070 ± 45 and 2160 ± 45 MeV.

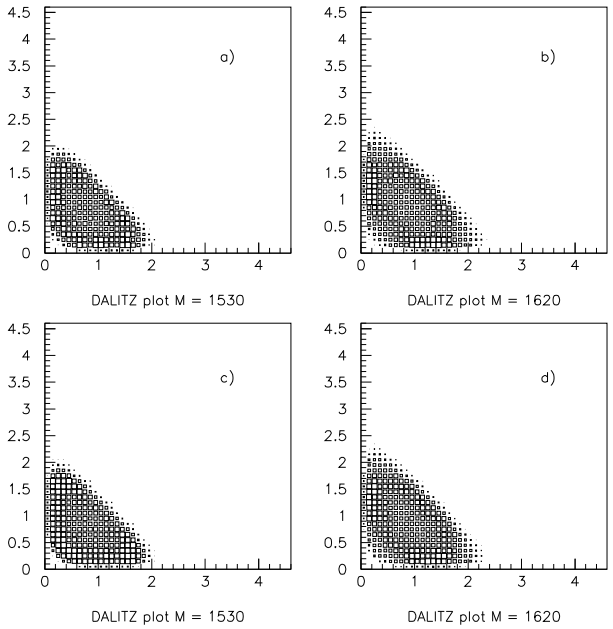

Fig.21. As Fig. 17 with $a_1(1640)$ excluded from the fit.

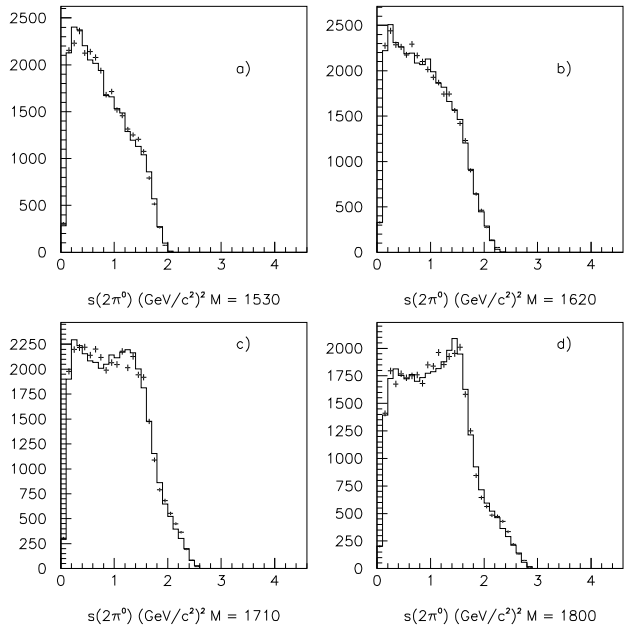

Fig.22 The 2π mass^2 spectrum projected from Figs. 17 and 18.

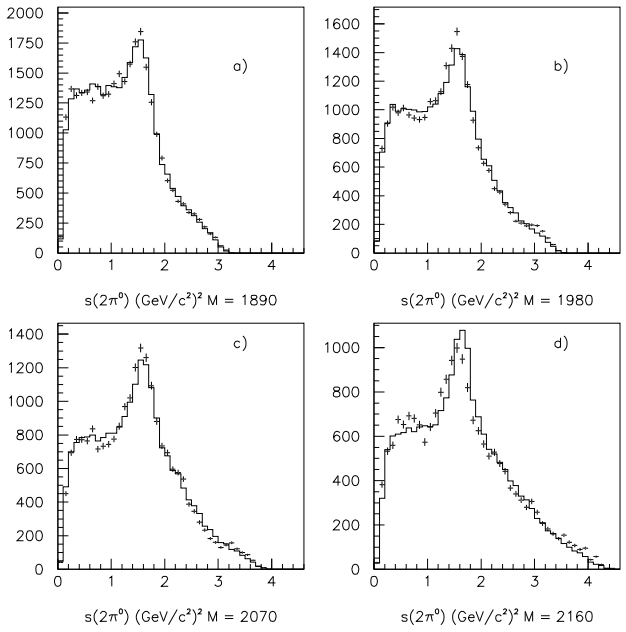

Fig.23 The 2π mass^2 spectrum projected from Figs. 19 and 20.

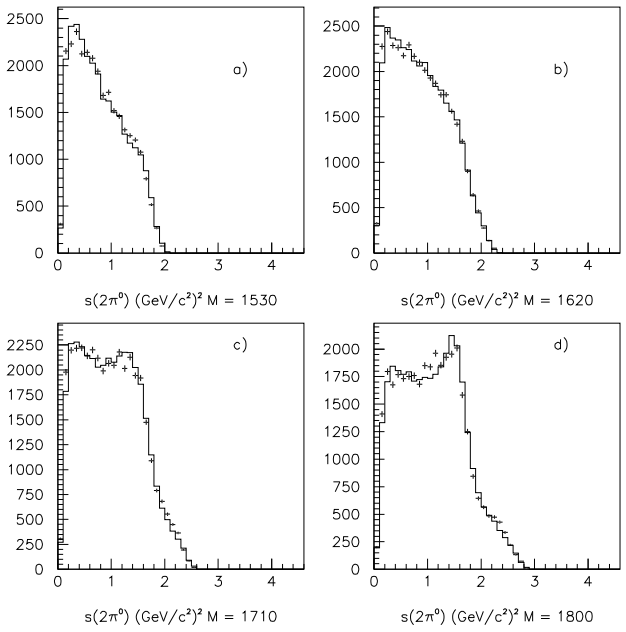

Fig.24 The 2π mass^2 projection with $a_1(1640)$ excluded from the fit.

10 Summary

There really does seem to be a 1^+ resonance around 1640 MeV, though it has been arduous digging it out. It seems worth reporting it factually, despite the fact that it is not directly visible in mass projections and scatter plots. It seems unlikely the detector is misbehaving very badly. We see no reason why a fault should concentrate the signal into a narrow mass range around 1640 MeV; we would expect it to be spread over all masses. The signal is roughly a 14 standard deviation effect statistically and is half as strong as the $\pi_2(1670)$ itself.

The evidence we have presented depends on (i) the mass scan, (ii) the correct angular dependence observed in two decay channels, and (iii) simulations of possible 'leakage' effects. It is disappointing that projections show no distinctive evidence for $a_1(1640)$, so it needs further confirmation elsewhere. The fit to the spectrum and scatter plots of Fig. 2 shows hardly any change when $a_1(1640)$ is included in the fit. It is therefore the angular dependence which is providing the evidence for its presence.

A radial excitation of $a_1(1260)$ is to be expected around 1650 MeV, and decay modes to $\sigma\pi$ and $f_2(1270)\pi$ are likely. There has been earlier evidence [7] for a $J^{PC} = 1^{++}$ resonance at 1650 MeV with $\Gamma \sim 400$ MeV, decaying to $\rho\pi$ with $L = 2$. [The absence of $L = 0$ $\rho\pi$ decays is predicted by Ted Barnes (private communication), because of a node in the radial wave function.] Daum et al. [8] also reported tentative evidence for a 1^{++} resonance near 1700 MeV in this channel. Lee et al. [9] presented evidence for a 1^{++} resonance with $I = 1$ around 1700 MeV in $f_1(1285)\pi$, but did not quote a value for its width.

The branching ratio between $\sigma\pi$ and $f_2(1270)\pi$ decays modes has been evaluated following the methods developed in our $5\pi^0$ paper [10]. From the coupling constants fitted to the data, we find, after integrating over the available phase space, a branching ratio:

$$\frac{BR(a_1(1640) \to f_2\pi)}{BR(a_1(1640) \to \sigma\pi)} = (24 \pm 7)\%. \tag{12}$$

If one includes all interferences amongst the 12 a_1 combinations, as in Table 1, this ratio changes to 27%.

For $\pi_2(1670)$ we find a ratio of decays to $f_2(1270)\pi$ with $L = 2$ and $L = 0$:

$$\frac{D}{S} = -0.18 \pm 0.06, \tag{13}$$

in agreement with the magnitude found by Daum et al. [8]: 0.22 ± 0.1; however, our data require destructive interference between these two decays. Daum et

al. do not quote the phase angle between the two decay modes.

We also find for $\pi_2(1670)$ the ratio of branching ratios:

$$\frac{BR(\pi_2 \to [\sigma\pi]_{L=2})}{BR(\pi_2 \to [f_2\pi]_{L=0})} = 0.24 \pm 0.1, \tag{14}$$

in agreement with Daum et al., who find 0.20 ± 0.10. If all interferences amongst the twelve π_2 combinations are included, as in Table 1, the ratio changes only to 0.30.

References

[1] J. Adomeit et al., Zeit. Phys. C71 (1996) 227.

[2] A. Zaitsev, Hadron'97 Proceedings.

[3] P. Eugenio, Ph.D. thesis.

[4] A. Abele et al. Nucl. Phys. B (to be published).

[5] B.S. Zou and D.V. Bugg, Phys, Rev. D48 (1993) 3948.

[6] Particle Data Group, Phys. Rev. D54 (1996) 1.

[7] J. Pernegr et al., Nucl. Phys. B134 (1978) 436.

[8] C. Daum et al., Nucl. Phys. B182 (1981) 269.

[9] J.H. Lee et al., Phys. Lett. B323 (1994) 227.

[10] A. Abele et al., Phys. Lett. B380 (1996) 453.